AIAA JOURNAL
Vol. 38, No. 9, September 2000

Model Attitude Determination in Wind Tunnel with a Luminescent Paint Data System

Wim Ruyten*
Sverdrup Technology, Inc., Arnold Air Force Base, Tennessee 37389-4300

The question is addressed how registration targets in luminescent paint images can be used to determine model position and attitude (P&A) of the test article in a wind-tunnel test. The theory for such P&A determinations is developed and applied to data from a pressure-sensitive paint test in Arnold Engineering Development Center's 16-ft Transonic Wind Tunnel. It is shown that the camera system is capable of resolving pitch and yaw angles to within 0.005 deg rms. However, systematic differences as large as ± 0.05 deg are found between the camera-based angles and angles determined from a sting-mounted balance. By analyzing the motion of the cameras relative to the tunnel walls, the observed discrepancies may be explained by rotation of the cameras relative to the test article. In some cases, these rotations are clearly correlated to operating conditions of the tunnel.

Nomenclature

$a_{c1} \cdots a_{c11}$	= camera calibration coefficients with respect to model coordinate system
$a^*_{c1} \cdots a^*_{c11}$	= camera calibration coefficients with respect to tunnel coordinate system
$f(t)$	= yaw history vs time
N_{tot}	= number of registration targets in least-squares sum
$R_{11} \cdots R_{33}$	= rotation matrix elements
U_{ci}, V_{ci}, W_{ci}	= quantities used in imaging equations
u_c, v_c	= image center for wall-rotation analysis
u_{ci}, v_{ci}	= image coordinates of registration target
u_i, v_i	= image coordinates of wall target
x_i, y_i, z_i	= model coordinates of registration target
x^*_i, y^*_i, z^*_i	= tunnel coordinates of registration target
α, β, ϕ	= pitch, yaw, roll of test article
β_{ck}	= camera yaw angle for camera k
β_{wk}	= wall yaw angle for camera k
$\Delta u, \Delta v$	= camera-wall displacement parameters
$\Delta u_i, \Delta v_i$	= image centroid shifts
$\Delta x, \Delta y, \Delta z$	= displacement of test article with respect to tunnel coordinate system
δ	= camera-wall rotation angle
σ_{rms}	= residual fit error
χ^2	= to-be-minimized error sum from Eq. (6)
χ^2_w	= to-be-minimized error sum from Eq. (7)

I. Introduction

Luminescent paint measurements are assuming an increasingly prominent role in aerodynamic testing.[1–3] This is especially true at the Arnold Engineering Development Center (AEDC), which has upgraded its pressure-sensitive paint (PSP) system for the 16-ft Transonic Wind Tunnel to one that employs eight cameras in the test section. To perform PSP measurements, a luminescent coating, whose luminescent yield under suitable illumination is a function of the pressure or temperature at the surface, is applied to a test article. By imaging the surface, it is thus possible to determine the pressure or temperature distribution on the test article. Most importantly, the PSP system is expected to reduce cycle time for test and development projects by providing faster and more comprehensive data than can be obtained by traditional techniques.

A common task in luminescent paint measurements is resection.[4–7] This is the process of mapping two-dimensional image data onto a three-dimensional grid of the test article. To accomplish this task, registration targets are placed on the test article. The desired mapping transformations are then inferred from the coordinates of these targets in three-dimensional object space and in two-dimensional image space. This process presents the interesting opportunity to use the image coordinates of the registration targets to calculate the position and attitude (P&A) of the test article optically. By contrast, traditional measurements of model attitude involve a complex procedure for combining and calibrating data from sting-mounted balance sensors and strain gauges. The accuracy of such measurements is estimated to be in the range of 0.02–0.05 deg. The motivation for the present study was to investigate the possibility of using the optical data system to improve these accuracies to 0.01 deg or better, as desired with increasing frequency by AEDC test customers.

The organization of this paper is as follows. In Sec. II, principles of optical P&A determination are formulated for the problem at hand. In Sec. III, these principles are applied to image data from three cameras that were used in a PSP test, i.e., before the upgrade to an eight-camera system. Section IV concludes with a comparison of the results achieved at AEDC with optical data obtained in wind tunnels elsewhere.[7–10]

II. Theory

Determination of model P&A parameters by optical means is a well-known problem in photogrammetry.[10–12] Consider the process of imaging a test article (the model) on which are placed a number of registration targets. Let (x_i, y_i, z_i) be the three-dimensional coordinates of these targets in a coordinate system that is tied to the model, and let (u_{ci}, v_{ci}) be the corresponding two-dimensional image coordinates for camera c. If lens distortion is neglected, the relation between these two sets of coordinates may be expressed as[4,5,10–15]

$$u_{ci} = U_{ci} / W_{ci}, \qquad v_{ci} = V_{ci} / W_{ci} \tag{1}$$

where

$$U_{ci} = a_{c1}x_i + a_{c2}y_i + a_{c3}z_i + a_{c4} \tag{2a}$$

$$V_{ci} = a_{c5}x_i + a_{c6}y_i + a_{c7}z_i + a_{c8} \tag{2b}$$

$$W_{ci} = a_{c9}x_i + a_{c10}y_i + a_{c11}z_i + 1 \tag{2c}$$

Here $a_{c1} \cdots a_{c11}$ are camera calibration coefficients. Equations (1) and (2) may be interpreted either as a direct linear transform or as a projective transform. In the first case, $a_{c1} \cdots a_{c11}$ are treated as independent parameters. In the second case, $a_{c1} \cdots a_{c11}$ are constrained by the interior and exterior coordinates of the camera.[10–15] In both cases, the coefficients $a_{c1} \cdots a_{c11}$ may be obtained by fitting measured values of the image coordinates (u_{ci}, v_{ci}) to a known set

Presented as Paper 99-0181 at the AIAA 37th Aerospace Sciences Meeting, Reno, NV, 11–14 January 1999; received 14 June 1999; revision received 12 January 2000; accepted for publication 21 January 2000.

*Engineer Specialist, Instrumentation and Diagnostics Branch, AEDC Group; wim.ruyten@arnold.af.mil. Senior Member AIAA.

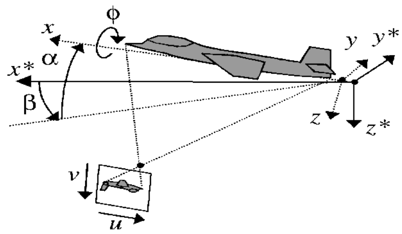

Fig. 1 Definition of coordinate systems.

of model coordinates (x_i, y_i, z_i). This is the standard approach for performing resection in luminescent paint measurements. Although adequate for mapping two-dimensional image data onto a three-dimensional grid, the resulting coefficients $a_{c1} \cdots a_{c11}$ provide little insight into the position and attitude of the test article, even though they depend on them.

In the alternative scheme considered here, a third coordinate system is introduced, namely that associated with the wind tunnel (see Fig. 1). The orientation of the test article, i.e., the model coordinate system, with respect to the tunnel coordinate system can now be expressed in terms of a displacement vector $(\Delta x, \Delta y, \Delta z)$ and a set of three Euler angles α, β, and ϕ. The relationship between the model coordinates (x_i, y_i, z_i) of a registration target and the associated tunnel coordinates (x_i^*, y_i^*, z_i^*) is then given by

$$\begin{pmatrix} x_i^* \\ y_i^* \\ z_i^* \end{pmatrix} = \begin{pmatrix} \Delta x \\ \Delta y \\ \Delta z \end{pmatrix} + \begin{pmatrix} R_{11} & R_{12} & R_{13} \\ R_{21} & R_{22} & R_{23} \\ R_{31} & R_{32} & R_{33} \end{pmatrix} \begin{pmatrix} x_i \\ y_i \\ z_i \end{pmatrix} \tag{3}$$

where[16]

$$R_{11} = \cos\alpha\cos\beta \tag{4a}$$

$$R_{12} = \sin\beta\cos\phi + \sin\alpha\cos\beta\sin\phi \tag{4b}$$

$$R_{13} = -\sin\beta\sin\phi + \sin\alpha\cos\beta\cos\phi \tag{4c}$$

$$R_{21} = -\cos\alpha\sin\beta \tag{4d}$$

$$R_{22} = \cos\beta\cos\phi - \sin\alpha\sin\beta\sin\phi \tag{4e}$$

$$R_{23} = -\cos\beta\sin\phi - \sin\alpha\sin\beta\cos\phi \tag{4f}$$

$$R_{31} = -\sin\alpha \tag{4g}$$

$$R_{32} = \cos\alpha\sin\phi \tag{4h}$$

$$R_{33} = \cos\alpha\cos\phi \tag{4i}$$

Now reinterpret the imaging equations from Eqs. (1) and (2) in terms of the tunnel coordinates (x_i^*, y_i^*, z_i^*). The result from Eqs. (2) can then be rewritten as

$$U_{ci} = a_{c1}^* x_i^* + a_{c2}^* y_i^* + a_{c3}^* z_i^* + a_{c4}^* \tag{5a}$$

$$V_{ci} = a_{c5}^* x_i^* + a_{c6}^* y_i^* + a_{c7}^* z_i^* + a_{c8}^* \tag{5b}$$

$$W_{ci} = a_{c9}^* x_i^* + a_{c10}^* y_i^* + a_{c11}^* z_i^* + 1 \tag{5c}$$

Asterisks in Eqs. (5) indicate that the coordinates and camera calibration coefficients are expressed with respect to the tunnel coordinate system. By combining Eqs. (1–5), an explicit expression may be obtained for the image coordinates (u_{ci}, v_{ci}) in terms of the model coordinates (x_i, y_i, z_i), the camera calibration coefficients $a_{c1}^* \cdots a_{c11}^*$, and the model P&A parameters Δx, Δy, Δz, α, β, and ϕ. Given the image coordinates of a sufficiently large set of targets, it is possible to determine the unknown parameters by minimizing the least-squares sum

$$\chi^2 = \sum_{c,i} \left\{ (u_{ci} - \tilde{u}_{ci})^2 + (v_{ci} - \tilde{v}_{ci})^2 \right\} \tag{6}$$

In Eq. (6), tildes are used to distinguish the measured image coordinates from the predicted ones. As indicated, the sum in Eq. (6) may include image coordinates from multiple cameras. The model coordinates (x_i, y_i, z_i) are presumed known through the use of a digitizing measurement arm. Minimization of Eq. (6) may thus be used either for calibrating the camera coefficients $a_{c1}^* \cdots a_{c11}^*$ for a known set of model P&A parameters, or for determining model P&A parameters once the coefficients $a_{c1}^* \cdots a_{c11}^*$ are known. In both cases, minimization of χ^2 requires an iterative algorithm. A simplex algorithm[17] was used in this work. (In subsequent work it has been shown that a more efficient iteration may be obtained by use of the Levenberg–Marquardt method, which offers the additional advantage of yielding estimates of the precision of the fit parameters.[18,19]) Starting values for the fit parameters were obtained by first minimizing the error sum

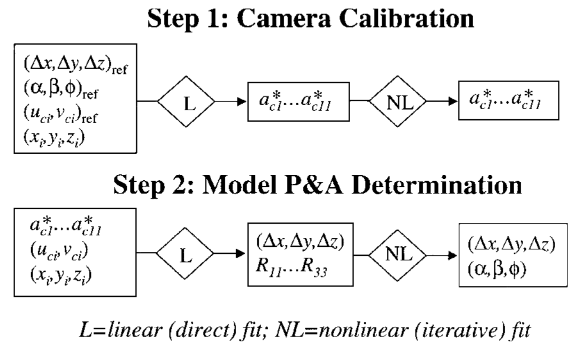

Fig. 2 Processing steps.

$$\chi_w^2 = \sum_{c,i} \left\{ (U_{ci} - \tilde{u}_{ci} W_{ci})^2 + (V_{ci} - \tilde{v}_{ci} W_{ci})^2 \right\} \tag{7}$$

which is obtained from Eq. (6) by multiplying the terms in parentheses by the terms W_{ci} from Eq. (5c). Substituting the results from Eqs. (3) and (5) into Eq. (7) yields an expression for χ_w^2 that is quadratic in the camera coefficients $a_{c1}^* \cdots a_{c11}^*$, in the model position parameters $(\Delta x, \Delta y, \Delta z)$, and in the nine elements $R_{11} \cdots R_{33}$ of the test article rotation matrix. Setting to zero the derivatives of this expanded form of Eq. (7) with respect to the unknown parameters leads to a system of linear equations from which may be found, in the case of camera calibration, the coefficients $a_{c1}^* \cdots a_{c11}^*$ (by solving 11 equations) or in the case of model P&A determination, the 12 P&A parameters from Eq. (3) (by solving 12 equations). At least six coordinate pairs $(\tilde{u}_{ci}, \tilde{v}_{ci})$ are required in either case for these equations to have a unique solution. From these parameters, starting values for the iterative minimization of Eq. (6) may be constructed.

Figure 2 shows a flowchart of the resulting fitting processes. Camera calibration and model P&A determination are shown as separate processes. Both involve a linear step to obtain starting values for the fit parameters and an iterative step for their optimization. In all cases, the preeminent measure for the quality of the resulting fits is the rms deviation, in pixels, between fitted and measured image coordinates given by

$$\sigma_{\mathrm{rms}} = \left(\chi^2 / N_{\mathrm{tot}}\right)^{\frac{1}{2}} \tag{8}$$

where N_{tot} is the total number of image coordinate pairs in the sum χ^2 from Eq. (6).

The P&A determination technique described here differs from techniques used in stereo-photogrammetry because it is not necessary to obtain explicit values for the tunnel coordinates (x_i^*, y_i^*, z_i^*) of the registration targets. The technique can be used with a single camera and offers the opportunity to combine measurements from multiple cameras even if their fields of view do not overlap. These advantages derive from the fact the relative locations of the registration targets are known through the use of a digitizing measurement arm.

III. Application to Wind Tunnel Data

The theory from Sec. II is now applied to image data from a PSP test in AEDC's 16-ft Transonic Wind Tunnel. The test was performed on a 1:10 scale model of a German Dornier Alpha jet,

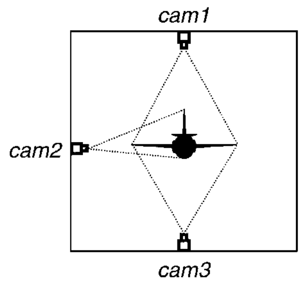

Fig. 3 Experimental setup.

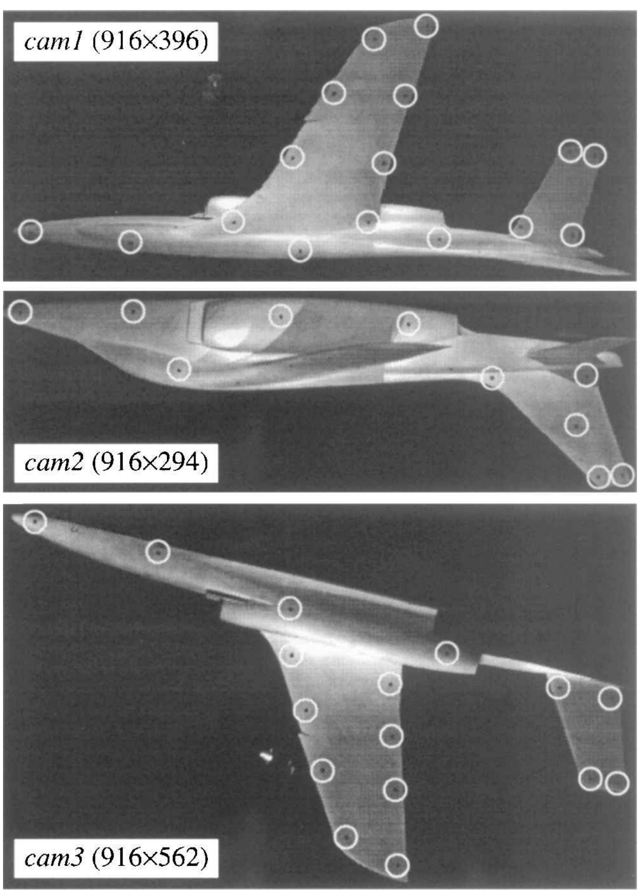

Fig. 4 PSP images of TST model at wind-off test point 16301.

known as the TST model.[20,21] Nominal pitch angles in the test were 0, 2, 4, 5, and 6 deg. No intentional yaw or roll angles were introduced. Registration targets were placed only on the painted right half of the model. Three 1024 × 1024 × 16-bit charge-coupled device (CCD) cameras were used, as shown in Fig. 3. Figure 4 shows representative images from the three cameras. Registration targets (white circles) and image sizes, in pixels, are indicated. Camera focal lengths were in the range 50–60 mm, with aperture settings of f/8. Image exposure times were in the range 1–3 s.

The registration targets consisted of black circular dots, with diameters of 6.4 mm in model space, or about five image pixels in image space for all three cameras. This is about the optimum target size (4–6 pixels) for PSP measurements; slightly larger targets (6–8 pixels) would be preferred for model attitude measurements per se.[8] Of the forty-two registration targets on the model, only those that were viewed less than 30 deg off-normal were used. Thus, 10 targets were used in conjunction with the side-mounted camera and 16 targets each were used in conjunction with the top- and bottom-mounted cameras. Larger off-normal viewing angles may be used, as long as the minimum width of an imaged target is at least several pixels.

A total of 344 images was used for P&A analysis: 90 for the side-mounted camera, 127 each for the top- and bottom-mounted cameras. Image coordinates of the registration targets were calculated by the PSP analysis program using an intensity-weighted centroiding algorithm with baseline offset.[22] Analysis of the data was focused on two tasks: determination of pitch angles from the side-mounted camera, and determination of yaw angles from, separately, the top- and bottom-mounted cameras. Traditional values for pitch, yaw, and roll of the model were also available from digital angle sensors and strain gauges on a sting-mounted balance. These angles include corrections for sting deflections under dynamic loading and are believed to be accurate to about 0.02–0.03 deg. All pitch angles quoted here exclude a Mach-number-dependent flow-angle correction (a number in the range 0 to −0.26 deg), which cannot be measured optically. No flow-angle corrections were considered for yaw.

A. Calibration and Data Analysis

The model xyz coordinates were determined in five steps. First, the TST model was positioned at 0-deg pitch, yaw, and roll. Second, to calibrate the digitizing measurement arm, the tip of the arm was placed on selected pressure taps whose three-dimensional coordinates were assumed to be those from an engineering drawing of the TST model. Third, having established a coordinate system for the measurement arm in this way, the xyz model coordinates of the registration targets on the top of the model and the fuselage were measured. Fourth, to access the targets on the bottom of the model, the model was rolled over 180 deg and the second and third steps were repeated. Fifth, the model coordinates of the registration targets were fine-tuned using the back-projection method from Ref. 23, which uses image coordinates from a series of luminescent paint images to update the model coordinates as measured with the digitizing measurement arm.

To define the tunnel coordinate system $x^*y^*z^*$ from Fig. 1, wind-off test point 16301 was selected as a reference. At this point, yaw and roll angles were assumed to be zero by definition. The pitch angle was taken to be equal to the value reported by the wind-tunnel data system (−0.09 deg). The position of the test article, $(\Delta x, \Delta y, \Delta z)$, was defined to be $(0, 0, 0)$ at this point. At the reference point, the tunnel coordinates (x_i^*, y_i^*, z_i^*) of all 42 registration targets could thus be calculated using Eqs. (3) and (4), allowing calibration of the camera coefficients $a_{c1}^* \cdots a_{c11}^*$. One consequence of a single-point calibration of this sort is that any deviation between actual and assumed angles at the calibration point introduces a bias error in the definition of the tunnel coordinate system. An example of such a bias error is encountered in Sec. III.C, in which a roll misalignment on the order of 0.5 deg is identified between the assumed and actual pitch planes of the model support system. In Ref. 18, a multipoint calibration procedure is described that may be used to mitigate the introduction of such bias errors.

Projective transform equations were used for both camera calibration and P&A determination. Following determination of the coefficients $a_{c1}^* \cdots a_{c11}^*$ for each camera, model P&A parameters were determined for all images by successive minimization of Eqs. (7) and (6). Residual fit errors from Eq. (8) were about 0.09 pixels rms for all three cameras.

B. Pitch Angle Results

Image data from the side-mounted camera (cam2) were used to calculate model pitch. The results are plotted in Fig. 5 as a function of image sequence number. In this format, the data merely reveal the 0- to 6-deg range of pitch angles used in the test. To assess the accuracy of the data, Fig. 5 also shows the differences between the camera-based pitch angles and the pitch angles that were derived from the wind tunnel balance. Differences in the range −0.06 to +0.06 deg are found, with an rms deviation from zero equal to 0.028 deg. These differences are surprisingly large and are clearly not randomly distributed. The big jump in pitch angle difference between the eighteenth and nineteenth data points coincides with a change from a wind-on condition to wind off. During this process, an adjustment had to be made to the cam2 camera. Thus, the large jump between the eighteenth and nineteenth data points may have been caused by bumping the camera. To check for this effect, the cam2 images were reanalyzed to check for rotation of the camera relative to the tunnel wall in the background of the cam2 images. As an example, Fig. 6 shows a greatly enhanced version of the cam2 image at the reference test point, point 16301 (cf. Fig. 4), in which holes and other features

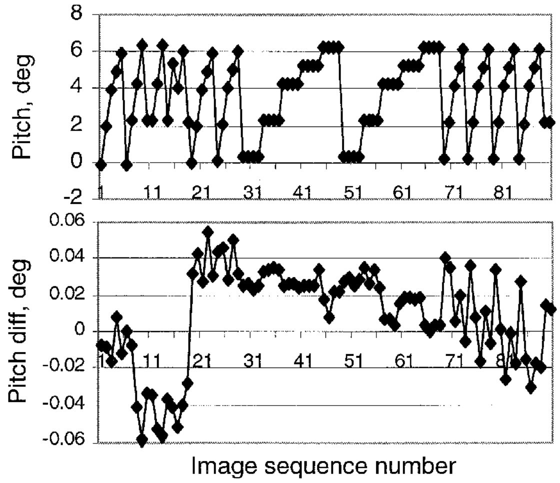

Fig. 5 History of pitch angles and pitch angle differences between cam2 data and balance-derived values.

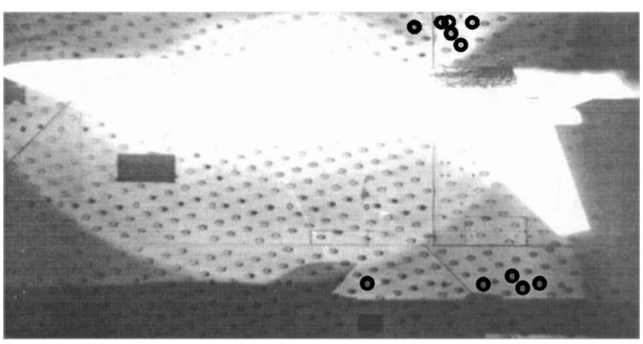

Fig. 6 View of tunnel wall opposite of cam2 camera. Circles indicate image features used for camera-wall rotation analysis.

in the perforated tunnel walls are clearly visible. Black circles indicate features that were selected to serve as registration targets. The image centroids of these features were calculated for all cam2 images. For each image separately, the centroids were then fitted to the expression

$$\begin{pmatrix}\Delta u_i\\ \Delta v_i\end{pmatrix} = \begin{pmatrix}\Delta u\\ \Delta v\end{pmatrix} + \begin{pmatrix}1 & -\delta\\ \delta & 1\end{pmatrix}\begin{pmatrix}u_i - u_c\\ v_i - v_c\end{pmatrix} \tag{9}$$

where Δu_i and Δv_i are the shifts in image coordinates of the ith feature in a given image relative to the reference image (at test point 16301), and $u_i - u_c$ and $v_i - v_c$ are the displacements of the image coordinates in the reference image from the image center. The three fit parameters in Eq. (9) are the image shifts Δu and Δv, and the image rotation angle δ, which is assumed to be small. Table 1 lists typical residual fit errors [cf. Eq. (8)] and image shifts, both in terms of image pixels and millimeter displacements relative to the tunnel wall. Most importantly, Fig. 7 shows δ as a function of image sequence number. Unmistakably, the same jump in pitch angle is found as that which is seen between the eighteenth and nineteenth points in Fig. 7. This indicates that the discrepancy between the camera-based pitch angles in Fig. 7 and the balance-derived values is based, at least in part, on motion of the cam2 camera.

In addition to the big jump between points 18 and 19, the rotation angles in Fig. 7 show a distinct correlation to tunnel Mach number, which is also shown in Fig. 7. Four of the five changes in Mach number are clearly reflected in the camera-to-wall rotation data. It does not follow that the wall is stationary and only the camera moves. As will be seen in Sec. III.C, it is in fact likely that the tunnel walls move as well. The rotation effect in Fig. 7 is likely a composite effect of camera motion and wall motion. As a result, the rotation angles from Fig. 7 do not necessarily account for all of the observed discrepancies between the cam2-based pitch angles and the balance-derived values in Fig. 5.

Table 1 Wall-camera displacement analysis for cam2

Parameter	Value
Number of images	90
Number of registration features	11
Fit error $\sigma_{\rm rms}$, pixels	0.15 to 0.25
Δu range, pixels	0.5 to −4.5
Δv range, pixels	0 to −2.5
Δu range, mm on wall	−2 to −12
Δv range, mm on wall	0 to −7

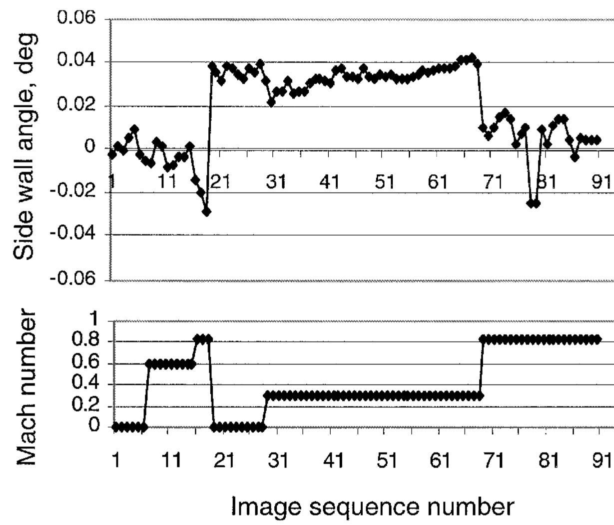

Fig. 7 History of observed wall rotation angles as seen by cam2, alongside tunnel Mach number.

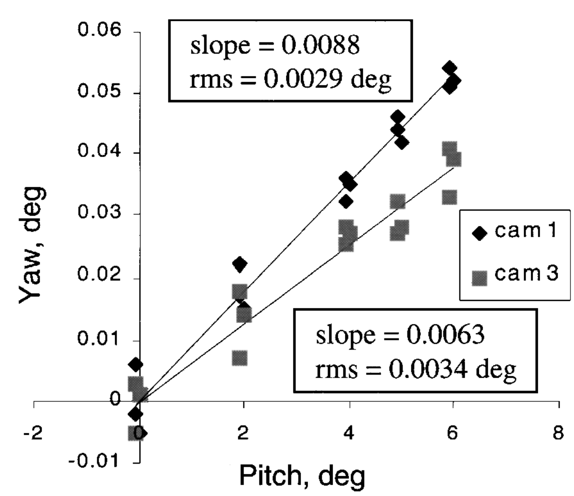

Fig. 8 Yaw vs pitch for wind-off data.

C. Yaw Angle Results

No deliberate yaw angles were introduced in the test. Still, the procedures from Sec. II were followed to determine yaw angles for the top- and bottom-mounted cameras. Yaw angles in the range of 0–0.1 deg were found. The direction of yaw is "nose to the left," or right wing swept forward, relative to the wind-off reference test point, point 16301. The observed yaw angles correlate strongly with model pitch. Figure 8 shows this correlation explicitly for the wind-off data. A linear dependence of yaw vs pitch is found for both cameras. This indicates that the true pitch axis of the tunnel is rolled with respect to the y^* axis of the assumed tunnel coordinate system in Fig. 1 by an angle whose tangent is given by the slope of the curve fits. Actually, different roll misalignment angles are found for the two cameras, namely 0.50 deg for cam1 and 0.36 deg for cam3. Apparently, this discrepancy traces back to the fact that two orientations of the TST model were used (see Sec. III.A) to measure the xyz model coordinates of the 42 registration targets. The

Table 2 Results of further wall displacement analysis

Parameter	Value	
	cam1	cam3
Number of images	127	127
Number of features	11	10
Fit error σ_{rms}, pixels	0.15 to 0.60[a]	0.15 to 0.25
Δu range, pixels	0 to −4.5	−1.5 to 3
Δv range, pixels	0 to −1	−0.5 to 2
Δu range, mm on wall	0 to −12	−4 to 8
Δv range, mm on wall	0 to −3	−1 to 5

[a]Residual fit errors can be reduced, without an appreciable change in the calculated rotation angles, to 0.22 pixels rms by including a fit coefficient to allow for thermal expansion of the tunnel wall in the flow direction.

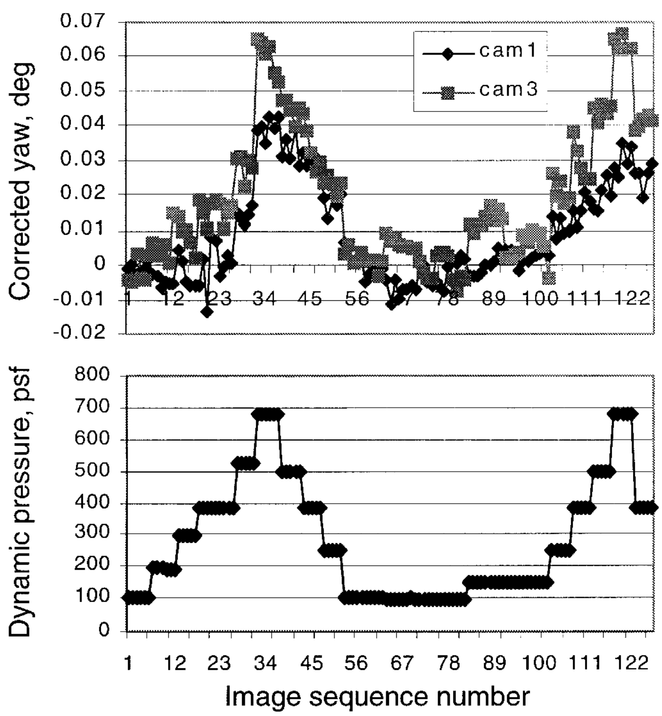

Fig. 9 Histories of pitch-corrected yaw and dynamic pressure.

data from Fig. 8 imply that the model coordinates of the targets on the top of the model (those imaged by cam1) are rolled relative to the bottom targets (those imaged by cam3) by the difference of the two misalignment angles, i.e., by 0.14 deg. In addition, Fig. 8 suggests that the model may have been mounted at a roll angle in the range of 0.36–0.50 deg relative to the true pitch axis of the wind tunnel.

Figure 9 shows a history of yaw angles for both wind-off and wind-on data points in which the measured yaw angles have been corrected for the misalignment effect from Fig. 8. Angles in the range of 0–0.06 deg remain. The corrected yaw angles correlate strongly to dynamic pressure ("Q"), which is shown in the bottom of Fig. 9. Such Q-dependent yaw effect would not be implausible in the presence of a sufficient side force or yawing moment on the model. However, yaw angles calculated from the measured side forces and yawing moments are less than 0.01 deg. It thus appears that the yaw angles in Fig. 9 may have to be interpreted in terms of camera motion.

To check for the existence of such camera motion, wall-to-camera rotation angles were calculated for all of the cam1 and cam3 images using the procedure described in Sec. III.B. Table 2 summarizes the fit results in the format from Table 1. Camera-to-wall rotation angles for both cam1 and cam3 are shown in Fig. 10. The two sets of data are almost identical, with an rms difference of only 0.007 deg. In addition, the camera-to-wall rotation angles in Fig. 10 are matched almost perfectly by the differences in the model yaw angles from cam1 and cam3 in Fig. 9. Allowing for a constant

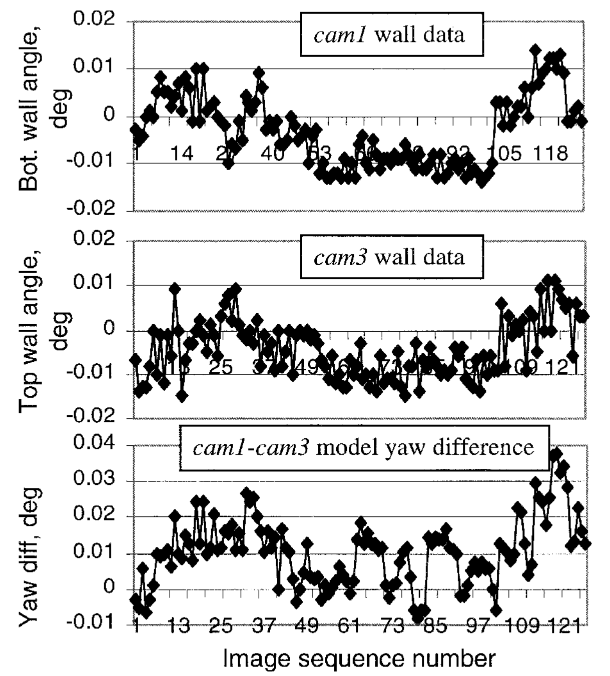

Fig. 10 Rotation angles for bottom and top tunnel walls, alongside model-based yaw-angle difference between top- and bottom-mounted cameras.

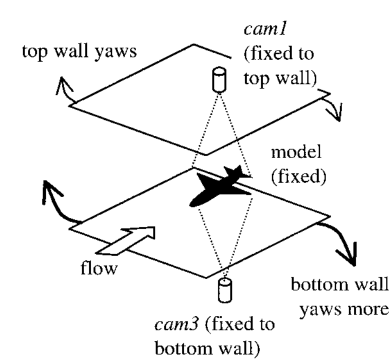

Fig. 11 Suggested mechanism for apparent model yaw with increasing dynamic pressure.

offset of 0.014 deg, this difference angle agrees with the average of the cam1 and cam3 camera-to-wall rotation angles in Fig. 10 to 0.0072 deg rms. The following argument can now be made to suggest that the top tunnel wall is yawing with respect to the bottom wall. Let $\beta_{c1}(t)$ and $\beta_{c3}(t)$ be the time-dependent yaw angles of the top and bottom cameras, respectively, relative to a presumed absolute reference system. Likewise, let $\beta_{w1}(t)$ and $\beta_{w3}(t)$ be the time-dependent yaw angles of the top and bottom walls. Then the three sets of data in Fig. 10 may be thought of as defining the following three relationships between these angles:

$$\beta_{c1}(t) - \beta_{w3}(t) = f(t) \tag{10a}$$

$$\beta_{w1}(t) - \beta_{c3}(t) = f(t) \tag{10b}$$

$$\beta_{c1}(t) - \beta_{c3}(t) = f(t) \tag{10c}$$

where $f(t)$ is the history of the three sets of data in Fig. 10. By combining Eqs. (10b) and (10c), it follows that $\beta_{c1}(t) = \beta_{w1}(t)$, i.e., the top camera yaws at the same rate as the top wall. Likewise, by combining Eqs. (10a) and (10c), it follows that $\beta_{c3}(t) = \beta_{w3}(t)$, i.e., the bottom camera yaws at the same rate as the bottom wall. Finally, by adding Eqs. (10a) and (10b) and subtracting Eq. (10c), it follows that $\beta_{w1}(t) - \beta_{w3}(t) = f(t)$, i.e., the top wall and the bottom wall yaw relative to each other. Because the model itself does not yaw (as follows from the force and moment data), it thus follows that the Q-dependent yaw effects in Fig. 9 are those of the top and bottom walls of the tunnel, with the bottom wall displaying the largest amount of yaw. This effect is illustrated in Fig. 11.

IV. Conclusions

The results from Sec. III suggest that a more rigorous mounting scheme is desirable for the CCD cameras if these are to be used for determining model pitch and yaw angles with an absolute accuracy of 0.01 deg or better. This will not be an easy task if the whole structure of the test cell flexes under dynamic and thermal loading, as is suggested by the data from Sec. III. Such flexing may not be easy to resolve and would have equal impact on other optical attitude measurement systems. Independent measurements of camera motion, e.g., through the use of gravity-sensing accelerometers, are desirable to resolve remaining ambiguities.

On the positive side, the data from Sec. III suggest that the sensitivity of the pitch- and yaw-angle determinations is on the order of 0.005 deg rms or better. For example, the residual fit errors in the yaw-vs-pitch curve fits from Fig. 8 are 0.0029 deg rms for the cam1 data and 0.0034 deg rms for the cam3 data. Also, the differences of 0.007 deg rms for the three sets of curves in Fig. 10 imply random errors in the individual rotation angle measurements of $0.007/\sqrt{2} = 0.005$ deg rms. Generally, 0.005 deg rms appears to be about the component of noise in most of the data from Sec. III. It thus appears that, if the problems caused by camera motion can be resolved, absolute measurements of model yaw and pitch with an accuracy of better than 0.01 deg rms should be possible. This was also confirmed by Monte Carlo simulation, as described in Ref. 23. The sensitivities of 0.003–0.005 deg rms for pitch and yaw determinations compare favorably with numbers quoted by other researchers. For example, in Refs. 7–9, resolutions in the range "sub-0.01" to 0.05 deg are quoted for the measurement of wing twist by optical means. A direct comparison is difficult, as the results depend on a host of factors, including camera optics, target size, target placement, and data processing.

Two possible sources of error that have not been considered are lens distortion in the imaging optics and model deformation at wind-on test conditions relative to wind-off conditions. In the case of lens distortion, correction terms need to be added to the imaging equations from Eq. (1).[10–14] These are accompanied by additional coefficients that need to be determined during the camera calibration process. Likewise, in the case of model deformation, additional terms can be added to Eq. (3) to account for a nonlinear dependence of the wind-on tunnel coordinates of registration targets on their wind-off model coordinates. The associated deformation coefficients then become additional fit parameters during the model P&A determination step from Fig. 2.

The inclusion of both lens distortion effects and model deformation effects in the theory from Sec. III warrants further study. For the TST test from Sec. III, both effects must have been small, given the small residual fit errors (0.09 pixels rms) between the predicted and measured coordinates of the registration targets.

A subtle point uncovered in this study is the practical difficulty of aligning the camera coordinate systems to the coordinate system of the wind tunnel. As demonstrated, yaw measurements during a pitch sweep may be used to calibrate roll angle misalignment of the tunnel pitch axis and the body y axis of the model. Likewise, roll measurements during a pitch sweep might be used to calibrate yaw angle misalignment of the pitch axis.

Improvements that are being contemplated for the AEDC optical data system include on-line data processing to provide position and attitude information in real time. A key element to such on-line processing is automatic image registration, as described in Ref. 22. Finally, P&A determinations are not limited to PSP tests. Rather, they should be applicable in most cases in which it is possible to place registration targets on the surface of the test article.

Acknowledgments

Discussions with my colleagues Daryl Sinclair, Marvin Sellers, David Cahill, and Frank Steinle are greatly appreciated. The TST program was conducted under a Memorandum of Understanding between the U.S. Air Force and the German Ministry of Education, Science, Research, and Technology (BMBF). Permission to publish images from the TST test was granted by Egon Stanewsky for BMBF. The author also wishes to acknowledge discussions with Tianshu Liu of High Technology Corporation (now at NASA Langley Research Center), Hampton, Virgina, for sharing insights into the applications of photogrammetry in wind tunnels.

References

[1]Kavandi, J., Callis, J., Gouterman, M., Khalil, G., Wright, D., Green, E., Burns, D., and McLachlan, B., "Luminescent Barometry in Wind Tunnels," *Review of Scientific Instruments*, Vol. 61, No. 11, 1990, pp. 3340–3347.

[2]Morris, M. J., Donovan, J. F., Kegelman, J. T., Schwab, S. D., Levy, R. L., and Crites, R. C., "Aerodynamic Applications of Pressure Sensitive Paint," *AIAA Journal*, Vol. 31, No. 3, 1993, pp. 419–425.

[3]McLachlan, B. G., and Bell, J. H., "Pressure-Sensitive Paint in Aerodynamic Testing," *Experimental Thermal and Fluid Science*, Vol. 10, No. 4, 1995, pp. 470–485.

[4]Bell, J. H., and McLachlan, B. G., "Image Registration for Luminescent Paint Sensors," AIAA Paper 93-0178, Jan. 1993.

[5]Bell, J. H., and McLachlan, B. G., "Image Registration for Pressure-Sensitive Paint Applications," *Experiments in Fluids*, Vol. 22, No. 1, 1996, pp. 78–86.

[6]Le Sant, Y., Deleglise, B., and Mebarki, Y., "An Automatic Image Alignment Method Applied to Pressure Sensitive Paint Measurements," *Proceedings of the 17th International Congress on Instrumentation in Aerospace Simulation Facilities*, edited by F. K. Owen, IEEE Publications, Piscataway, NJ, 1997, pp. 57–65.

[7]Bosnyakov, S., Bykov, A., Coulesh, V., Fonov, S., Morozov, A., Moskalik, V., Moskalik, L., Mosharov, V., Orlov, A., Radchenko, V., and Tarassov, N., "Blade Deformation and PSP Measurements on the Large Scale Rotor by Video Metric System," *Proceedings of the 17th International Congress on Instrumentation in Aerospace Simulation Facilities*, edited by F. K. Owen, IEEE Publications, Piscataway, NJ, 1997, pp. 95–103.

[8]Bell, J. H., and Burner, A. W., "Data Fusion in Wind Tunnel Testing; Combined Paint and Model Deformation Measurements," AIAA Paper 98-2500, June 1998.

[9]Burner, A. W., and Martinson, S. D., "Automated Wing Twist and Bending Measurements Under Aerodynamic Load," AIAA Paper 96-2253, June 1996.

[10]Liu, T., Radeztsky, R., Garg, S., and Cattafesta, L., "A Videogrammetric Model Deformation System and Its Integration with Pressure Sensitive Paint," AIAA Paper 99-0568, Jan. 1999.

[11]Wong, K. W., "Basic Mathematics of Photogrammetry," *Manual of Photogrammetry*, 4th ed., edited by C. C. Slama, American Society of Photogrammetry, Falls Church, VA, 1980, Chap. 2.

[12]McGlone, J. C., "Analytic Data Reduction Schemes in Non-Topographic Photogrammetry," *Non-Topographic Photogrammetry*, 2nd ed., edited by H. M. Karara, American Society of Photogrammetry and Remote Sensing, Falls Church, VA, 1989, Chap. 4.

[13]Cattafesta, L. N., III, and Moore, J. G., "Review and Application of Non-Topographic Photogrammetry to Quantitative Flow Visualization," AIAA Paper 96-2180, June 1996.

[14]Liu, T., Cattafesta, L. N., III, Radeztsky, R. H., and Burner, A. W., "Photogrammetry Applied to Wind-Tunnel Testing," *AIAA Journal*, Vol. 38, No. 6, 2000, pp. 964–971.

[15]Abdel-Aziz, Y. I., and Karara, H. M., "Direct Linear Transformation from Comparator Coordinates into Object Space Coordinates in Close-Range Photogrammetry," *Proceedings of the ASP/UI Symposium on Close-Range Photogrammetry*, Univ. of Illinois, Urbana, IL, 1971, pp. 1–18.

[16]Goldstein, H., *Classical Mechanics*, 2nd ed., Addison Wesley Longman, Reading, MA, 1980, p. 609.

[17]Caceci, M. S., and Cacheris, W. P., "Fitting Curves to Data," *Byte*, May 1984, pp. 340–362.

[18]Ruyten, W., "Model Attitude Measurement with an Eight-Camera Pressure-Sensitive Paint System," AIAA Paper 2000-0831, Jan. 2000.

[19]Press, W. H., Teukolsky, S. A., Vetterling, W. T., and Flannery, B. P., *Numerical Recipes in Fortran*, 2nd ed., Cambridge Univ. Press, New York, 1992, Chap. 15.

[20]Sellers, M. E., and Brill, J. A., "Demonstration Test of Pressure Sensitive Paint in the AEDC 16-ft Transonic Wind Tunnel Using the TST Model," AIAA Paper 94-2481, June 1994.

[21]Sellers, M. E., "Pressure Sensitive Paint Data on the Transonic Technology Wing Demonstrator (TST) in the AEDC Propulsion Wind Tunnel 16T," AEDC-TR-98-3, Tullahoma, TN, 1998.

[22]Ruyten, W., "Automatic Registration of Luminescent Paint Images," *Proceedings of the 45th International Instrumentation Symposium* (Albuquerque, NM), Instrumentation Society of America, Research Triangle Park, NC, 1999, pp. 279–288.

[23]Ruyten, W., "Toward an Integrated Optical Data System for Wind-Tunnel Testing," AIAA Paper 99-0181, Jan. 1999, Sec. 4.

R. P. Lucht
Associate Editor